Time-domain Analysis of a Polarization-Reconfigurable Ultra-Wideband Antenna in AFSIW Technology

Victor Van der Elst, Ruben Wilssens, Jelle Jocqué, Kamil Yavuz Kapusuz, Sam Lemey, Jo Verhaevert and Hendrik Rogier
Department of Information Technology, IDLab/Electromagnetics Group,
imec-Ghent University, Ghent, Belgium
Corresponding author email: victor.vanderelst@ugent.be

***Abstract*—This work presents the time-domain analysis of a compact polarization-reconfigurable Ultra-Wideband (UWB) antenna implemented in air-filled substrate-integrated waveguide (AFSIW) technology. This antenna is designed for operation in the IEEE-802.15.4z UWB channel 9 frequency band [7.74–8.24 GHz]. The proposed antenna utilizes a U-shaped slot within a quarter-mode AFSIW topology. Two PIN diodes enable +45°/-45° polarization switching by electrically shorting the slot at well-defined positions. Time-domain measurements demonstrate that the polarization-reconfigurable antenna exhibits negligible pulse distortion and virtually no phase-center variation, as confirmed by key UWB performance metrics: System Fidelity Factor (SFF) and Distance Estimation Error (DEE), particularly under varying orientations. It is demonstrated that a polarization-reconfigurable AFSIW antenna can be realized within a compact footprint of $0.6\lambda_0 \times 0.6\lambda_0$, achieving SFF values above 95% and DEE ≤ 3 cm over a 120° field of view. These characteristics make the antenna particularly well-suited for pulse-based UWB localization and sensing systems.**

***Index Terms*—Polarization-reconfigurable antenna, UWB, AFSIW, time-domain performance, system fidelity factor, SFF, distance estimation error, DEE**

I. Introduction

The Internet of Things (IoT) is transforming everyday environments by connecting billions of devices that continuously monitor and interact with their surroundings, especially in applications requiring real-time, location-aware services such as logistics, health monitoring, and smart infrastructure [1]. In indoor localization scenarios, where Global Navigation Satellite Systems (GNSSs) are often unavailable or unreliable, Impulse-Radio Ultra-Wideband (IR-UWB) technology stands out. It offers centimeter-level accuracy, strong resilience to multipath, and low interference thanks to the use of wide bandwidth (sub)nanosecond pulses [2]. UWB IoT nodes are often deployed in harsh environments, such as cluttered indoor spaces or mobile platforms, where reliable operation and high radiation efficiency are critical to maintain consistent communication and localization performance [3].

One key challenge in such systems is their vulnerability to polarization mismatch, which occurs when the transmitted and received signals are not aligned in polarization. This issue is problematic in time-domain applications where antenna orientation and indoor multipath conditions are unpredictable, leading to significant performance degradation [4].

To mitigate the impact of polarization mismatch, we recently proposed a Quarter-Mode (QM)-miniaturized Air-Filled Substrate-Integrated-Waveguide (AFSIW) antenna topology with polarization reconfigurability, operating in the 7.74–8.24 GHz band [5] and fully covering IEEE 802.15.4z UWB channel 9. This design achieves high radiation efficiency ($> 90\%$) while maintaining a compact footprint of $0.6\lambda_0 \times 0.6\lambda_0$. However, its performance has not yet been assessed in the time domain, which is critical for pulse-based UWB applications.

In this work, we present a comprehensive time-domain evaluation of this antenna, analyzing key UWB performance metrics, namely System Fidelity Factor (SFF) and Distance Estimation Error (DEE), for both linearly polarized (LP) states across a wide 120° field-of-view (FOV), with particular emphasis on varying orientations [3]. To the best of the authors' knowledge, this is the first time-domain characterization of a polarization-reconfigurable UWB antenna. The results show that the SFF remains above 90% in all measured cases over the entire 120° FOV, thereby satisfying the stringent SFF requirement. Moreover, the DEE results for all measured cases remain within ≤ 3 cm up to 120° FOV, demonstrating compliance with high-accuracy localization requirements.

Cavity-backed antennas implemented in AFSIW technology have emerged as promising candidates for IoT applications due to their cost-effective fabrication [6], [7], high efficiency, and wideband performance [8], [9]. To address the footprint constraints inherent to AFSIW structures [10], solutions such as capacitively loaded aperture-coupled stacked-patch configurations [11], [12] and QM-based Substrate-Integrated-Waveguide (SIW)/AFSIW miniaturization techniques [3], [13] have been proposed.

For high-precision localization and radar applications, antenna design must further prioritize time-domain performance metrics such as SFF and DEE, as they directly affect ranging and angle-of-arrival estimation accuracy. Recent work has demonstrated significant advances in system-level optimized UWB antennas [14], [15], explicitly targeting improvements in SFF and DEE to enhance localization performance.

Although wideband polarization-reconfigurable antennas based on AFSIW technology [16] and planar Printed Circuit Board (PCB) implementations [17] have shown great promise, their impact on system-level time-domain performance has not yet been comprehensively validated or optimized.

II. Polarization-Reconfigurable UWB Antenna

The polarization-reconfigurable antenna element (Fig. 1) presented in [5], utilizes a U-shaped slot within a QM-AFSIW topology. The U-shaped slot is divided in two L-shaped slots providing the corresponding +45° and -45° polarization states. Two PIN diodes enable switching of the L-shaped slot by electrically shorting it at well-defined positions. By controlling the states of the two PIN diodes (red and blue in Fig. 1), seamless switching between the $-45°$ and $+45°$ LP states is achieved. The $-45°$ state is obtained by forward-biasing the blue PIN diode with 1.35 V and 3 mA bias current while keeping the red PIN diode OFF, whereas the opposite bias configuration yields the $+45°$ state. Their DC bias is provided through inductive vias, which are isolated by capacitive gaps, allowing seamless bias-tee integration without additional lumped biasing components according to Fig. 1.

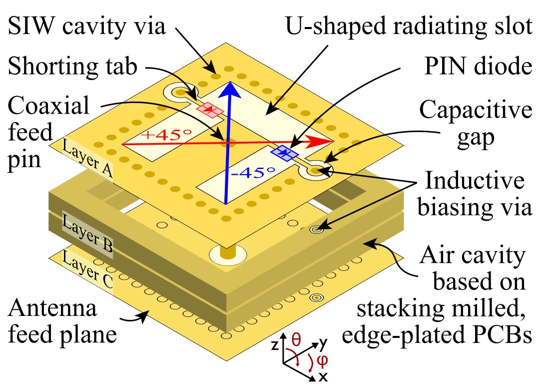

Fig. 1: Polarization-reconfigurable UWB antenna element in AFSIW technology. Two L-shaped slots combine into a single U-shaped slot with embedded PIN diodes to support polarization-reconfiguration.

Antenna prototypes are fabricated using a standard cost-effective PCB manufacturing process [18]. The antenna slot plane (layer A) and backplane (layer C) are implemented on a 0.254-mm-thick two-layer Rogers 4350B laminate [19], while the air cavity layers (layer B) are implemented through edge plating within a low-cost 3.24-mm-thick FR-4 dielectric laminate [20]. PIN diodes of type MA4AGBLP912 [21] by MACOM are chosen because of their low resistance (5.5 Ω) in their forward-biased state and low capacitance (5 fF) in their reverse-biased state. The chosen PIN diodes are soldered onto layer A.

Fig. 2 depicts the simulated and measured input reflection coefficients of the single element for both LP states, showing good agreement within the targeted IEEE802.15.4z channel 9. In both polarization states, the antenna maintains a 50 Ω match from 7.61 GHz to 8.20 GHz, achieving a -10 dB impedance bandwidth of 0.59 GHz (7.46%).

The radiation patterns of the single element are simulated and measured at the start, center and stop frequencies in the operating band, for both LP states. Fig. 3 shows the measured and simulated radiation patterns at 8 GHz, the center frequency of the operating band. This figure demonstrates strong agreement between simulation and measurement, with a maximum gain of 5.18 dBi at 28° from broadside. The variation of the far-field pattern in the IEEE 802.15.4z channel 9 frequency band is also shown in Fig. 3, represented using a lighter color tone. Each polarization state maintains a Half-Power Beamwidth (HPBW) exceeding 78°. The antenna achieves a boresight cross-polarization discrimination greater than 16.5 dB and a stable average boresight gain of 4.51 ± 0.76 dBi across the entire frequency band. In addition, the total antenna efficiency is 91% for both the $-45°$ and $+45°$ LP states.

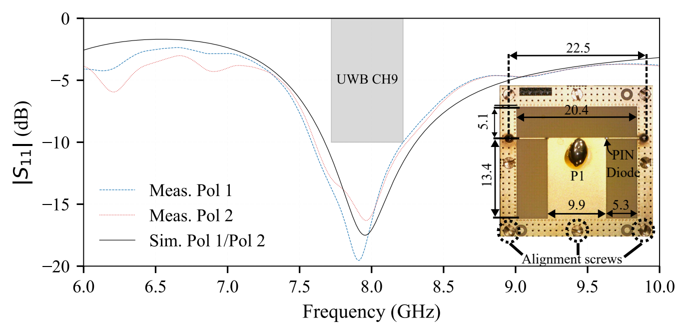

Fig. 2: Reflection coefficient $|S_{11}|$ of stand-alone antenna element in both operating states compared to the simulated results, with the gray area indicating the IEEE-802.15.4z UWB channel 9 band. The fabricated prototype is shown in the embedded figure with all relevant dimensions indicated in mm.

III. Time-domain analysis

To facilitate robust and reliable pulse-based operation, IR-UWB antennas must exhibit minimal orientation-dependent pulse distortion and phase-center variation. These properties are captured by the SFF, quantifying pulse fidelity, and the DEE, which expresses the impact on ranging accuracy. A low SFF or high DEE will degrade the communication link and ranging accuracy, reduce detection reliability and range, and can ultimately compromise the performance of the communication, localization or radar system [22], [23]. Consequently, the antenna's UWB performance is evaluated through comprehensive system-level analysis across a 120° FOV, employing time-domain measurements to assess the SFF and DEE as a function of θ.

In practical UWB systems, an SFF of at least 80% is generally acceptable, while precision-oriented applications typically require values above 90% [22]. When the SFF falls below 50%, pulse distortion becomes severe enough that the

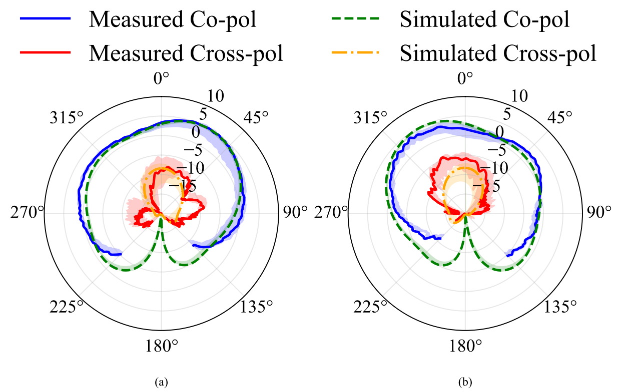

Fig. 3: Measured and simulated realized gain (dBi) at 8 GHz, with variation of the far-field pattern in the IEEE 802.15.4z channel 9 frequency band represented using a lighter color tone: (a) polarization 1 along the ϕ = -45°-plane and (b) polarization 2 along the ϕ = +45°-plane.

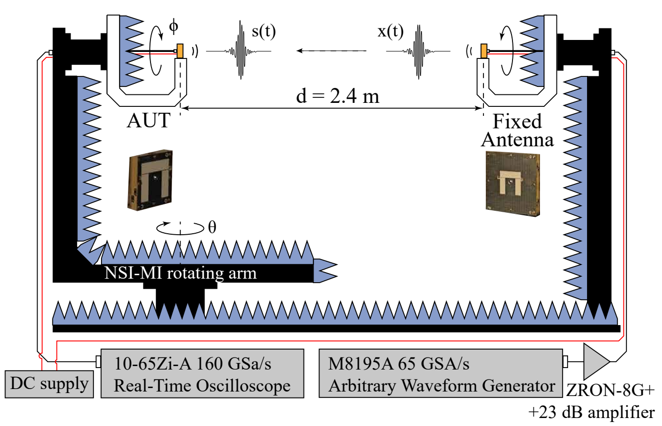

Fig. 4: Measurement setup in an anechoic room for system-level analysis of the proposed polarization-reconfigurable UWB antenna.

receiver can no longer reliably recognize the signal [24]. DEE is defined as the orientation-specific biasing error. In UWB systems, a DEE $\leq$ 3 cm is generally considered acceptable for accurate localization [3].

A representative UWB link is established using two polarization-reconfigurable IR-UWB antenna elements, following the procedure in [22]. Dedicated measurements are conducted using the NSI-MI spherical system inside an anechoic chamber, with the antennas separated by 2.4m, corresponding to a 7.98ns propagation delay. In this setup, the transmit antenna remains fixed, while the receive antenna – referred to as the Antenna Under Test (AUT) – is mounted on a rotating arm, as illustrated in Fig. 4. The signal applied to the fixed antenna consists of a standard modulated root-raised-cosine pulse $x(t)$, as defined in [25], with f_0 = 8 GHz as the carrier frequency and T_p = 2 ns as the pulse width, resulting in an effective bandwidth of 499.2 MHz [22]. The input pulse is generated by a Keysight M8195A Arbitrary Waveform Generator (AWG) operating at a sampling rate of 65 GSa/s, while the received pulses are captured with a Teledyne LeCroy LabMaster 10-65Zi-A Real-Time Oscilloscope (RTO), sampling at 160 GSa/s. A DC power supply is employed to bias the PIN diodes, enabling polarization reconfiguration. Proper biasing is achieved by applying a forward voltage of 1.35 V and supplying a current of 3 mA [5].

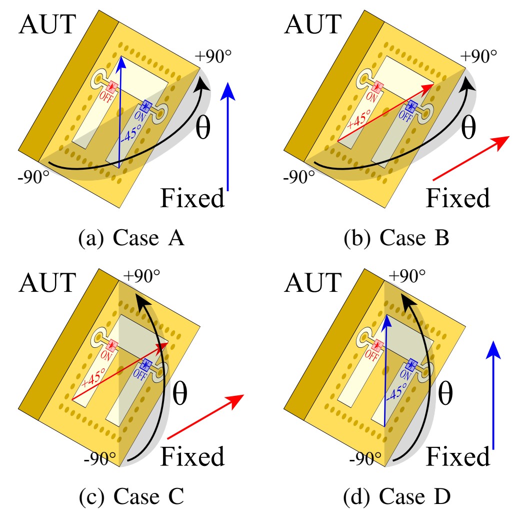

Fig. 5: Four different co-polarization cases measured.

The AUT was evaluated under four different co-polarization configurations. In all cases shown in Fig. 5, the AUT and the fixed antenna were aligned in co-polarization at $\theta = 0°$. The polarization state of both antennas could be set to either $-45°$ (blue arrow) or $+45°$ (red arrow).

Specifically, in Fig. 5 cases A and C, θ was rotated orthogonally with respect to the polarization direction, whereas in Fig. 5 cases B and D, θ was rotated along the polarization direction. Cases A and D correspond to the $-45°$ polarization state, and cases B and C correspond to the $+45°$ polarization state.

IV. Results and Discussion

We begin by presenting the measured transmitted and received UWB channel 9 pulse, which serves as the basis for understanding the subsequent experimental observations. Fig. 6 shows the normalized amplitude of the measured input pulse and the measured output pulse at broadside for case A, with markers indicating the 7.98 ns delay, corresponding to the 2.4 m distance between the antennas.

For the free-space link, the SFF is analyzed for all co-polarization cases in Fig. 7. Rotating θ as is shown in cases B and D of Fig. 5, demonstrates that the antenna meets the stringent requirement of SFF exceeding 95% across the entire $-60°$ to $+60°$ FOV. In cases A and C, the SFF remains above 90% for angles up to 120° FOV and above 95% for angles up from $-50°$ to $+33°$ FOV. This slight deviation results from the phase difference introduced when the two slots forming the linear polarization are rotated over

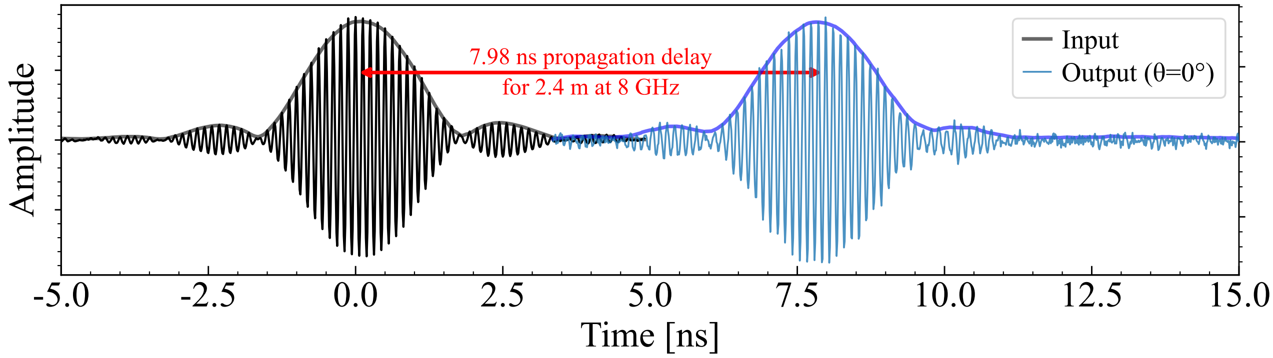

Fig. 6: Normalized amplitude of the measured input pulse and the measured output pulse at broadside, with markers showing the 7.98 ns delay, corresponding to the 2.4 m distance between the antennas.

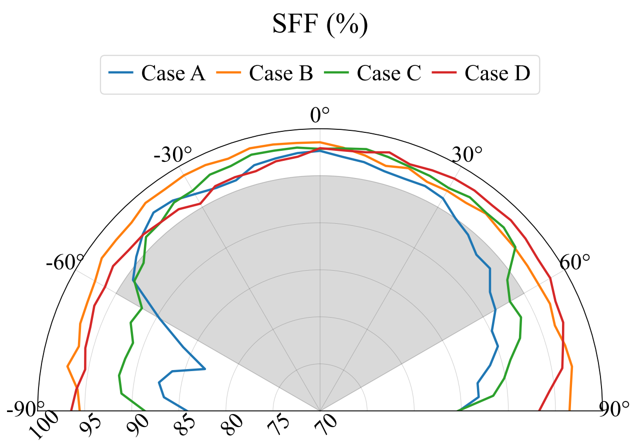

Fig. 7: Measured System Fidelity Factor (SFF) for the four co-polarization cases.

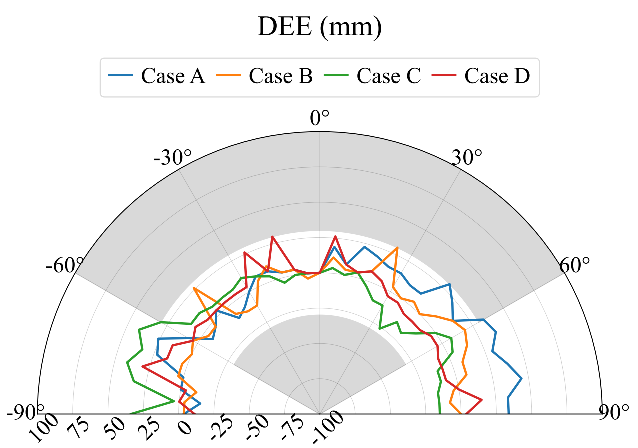

Fig. 8: Measured Distance Estimation Error (DEE) for the four co-polarization cases.

θ, causing one slot to exhibit a larger phase delay relative to the fixed antenna and resulting in imperfect co-polarization. Even under these conditions, the antenna remains well-suited for UWB systems, as the SFF remains above 90% across the entire $120°$ FOV, thereby ensuring compliance with SFF requirements.

With the proposed polarization-reconfigurable antenna, a fully cross-polarized state can be completely avoided, and therefore any drops in SFF need not be experienced in practice.

Beyond the SFF analysis, the DEE is evaluated to quantify the angle-dependent ranging bias introduced by the antenna link. Fig. 8 presents the DEE results for the four co-polarization cases, demonstrating that the stringent requirement of ≤ 3 cm is satisfied up to a FOV of $120°$.

V. Conclusion

The paper presents a thorough measurement campaign using the channel 9 UWB pulse, as defined in the IEEE802.15.4z standard. The proposed polarization reconfigurable antenna is analysed over a field-of-view of $120°$ and both polarization states were verified. The antenna performs within the stringent requirements for time-domain UWB systems.

References

[1] G. Pettorru, V. Pilloni, and M. Martalò, "Trustworthy Localization in IoT Networks: A Survey of Localization Techniques, Threats, and Mitigation," *Sensors*, vol. 24, no. 7, p. 2214, 2024.

[2] S. G. Leitch, Q. Z. Ahmed, W. B. Abbas, M. Hafeez, P. I. Laziridis, P. Sureephong, and T. Alade, "On Indoor Localization Using WiFi, BLE, UWB, and IMU Technologies," *Sensors*, vol. 23, no. 20, p. 8598, 2023.

[3] G.-J. Gordebeke, S. Lemey, O. Caytan, M. Boes, J. Jocqué, S. Van de Velde, C. Marshall, E. De Poorter, and H. Rogier, "Time-Domain-Optimized Antenna Array for High-Precision IR-UWB Localization in Harsh Urban Shipping Environments," *IEEE Sensors Journal*, vol. 24, no. 5, pp. 5561–5577, 2024.

[4] M. Naseri, A. Shahid, G.-J. Gordebeke, S. Lemey, M. Boes, S. Van De Velde, and E. De Poorter, "Machine Learning-Based Angle of Arrival Estimation for Ultra-Wide Band Radios," *IEEE Communications Letters*, vol. 26, no. 6, pp. 1273–1277, 2022.

[5] V. Van der Elst, K. Y. Kapusuz, S. Lemey, J. Verhaevert, and H. Rogier, "Compact Polarization-Reconfigurable AFSIW Array with Integrated Biasing Network," 2025, Manuscript accepted for publication in AEU - International Journal of Electronics and Communications.

[6] F. Parment, A. Ghiotto, T.-P. Vuong, J.-M. Duchamp, and K. Wu, "Air-Filled Substrate Integrated Waveguide for Low-Loss and High Power-Handling Millimeter-Wave Substrate Integrated Circuits," *IEEE Transactions on Microwave Theory and Techniques*, vol. 63, no. 4, pp. 1228–1238, 2015.

[7] L. Li and J.-B. Yan, "A Low-Cost and Efficient Microstrip-Fed Air-Substrate-Integrated Waveguide Slot Array," *Electronics*, vol. 10, no. 3, p. 338, 2021.

[8] Z. Xu, J. Liu, S. Huang, and Y. Li, "Gain-enhanced SIW cavity-backed slot antenna by using TE410 mode resonance," *AEU - International Journal of Electronics and Communications*, vol. 98, pp. 68–73, 2019.

[9] B. Wang, Z. Zhao, K. Sun, T. Tao, X. Yang, and D. Yang, "Low-Profile High-Aperture-Efficiency Air-Filled Substrate Integrated Cavity Antenna Array," *IEEE Antennas and Wireless Propagation Letters*, vol. 21, no. 7, pp. 1442–1446, 2022.

[10] S. A. Ali, M. Wajid, A. Kumar, and M. Shah Alam, "Design Challenges and Possible Solutions for 5G SIW MIMO and Phased Array Antennas: A Review," *IEEE Access*, vol. 10, pp. 88 567–88 594, 2022.

[11] I. Lima de Paula, S. Lemey, D. Bosman, Q. V. den Brande, O. Caytan, J. Lambrecht, M. Cauwe, G. Torfs, and H. Rogier, "Cost-Effective High-Performance Air-Filled SIW Antenna Array for the Global 5G 26 GHz and 28 GHz Bands," *IEEE Antennas and Wireless Propagation Letters*, vol. 20, no. 2, pp. 194–198, 2021.

[12] M. K.n. and Y. K. Choukiker, "Dual-mode aperture-coupled patch resonator based dual-band higher-order frequency selective surfaces," *AEU - International Journal of Electronics and Communications*, vol. 177, p. 155171, 2024.

[13] T. Wu, Z. Zhang, W.-j. Wang, and M.-j. Wang, "Coupling suppression study of miniaturized BDS/GPS multifunctional transceiver antenna based on quarter-mode substrate integrated waveguide," *AEU - International Journal of Electronics and Communications*, vol. 158, p. 154461, 2023.

[14] G.-J. Gordebeke, S. Lemey, and H. Rogier, "Metal-Stamped and IR-UWB-Optimized Air-Filled Cavity-Backed Antenna Array for Cost-Effective Single-Anchor 3D Localization," *IEEE Access*, vol. 13, pp. 125 016–125 028, 2025.

[15] Q. V. den Van den Brande, S. Lemey, and H. Rogier, "Planar Sectoral Antenna for IR-UWB Localization With Minimal Range Estimation Biasing," *IEEE Antennas and Wireless Propagation Letters*, vol. 20, no. 2, pp. 135–139, 2021.

[16] K. Y. Kapusuz, S. Lemey, and H. Rogier, "Multipolarization-Reconfigurable Air-Filled Substrate Integrated Waveguide Cavity-Backed Slot Antenna," *IEEE Antennas and Wireless Propagation Letters*, vol. 20, no. 4, pp. 622–626, 2021.

[17] Y. Wang, M. Ao, J. Su, Q. Guo, and Z. Li, "An ultra-wideband triple-polarization reconfigurable Vivaldi array antenna," *AEU - International Journal of Electronics and Communications*, vol. 188, p. 155575, 2025.

[18] "Making a PCB - PCB Manufacture Step-by-Step." [Online]. Available: https://34.252.181.249/making-a-pcb-pcb-manufacture-step-by-step/

[19] "RO4350B™ Laminates." [Online]. Available: https://rogerscorp.com/advanced-electronics-solutions/ro4000-series-laminates/ro4350b-laminates

[20] "IS400 Laminate and Prepreg." [Online]. Available: https://www.isola-group.com/pcb-laminates-prepreg/is400-laminate-and-prepreg-isola-group/

[21] "MA4AGBLP912." [Online]. Available: https://www.macom.com/products/product-detail/MA4AGBLP912

[22] J. Jocqué, Q. Van den Brande, S. Luchie, B. Van Herbruggen, E. De Poorter, J. Verhaevert, S. Lemey, P. Van Torre, and H. Rogier, "Resource-efficient simulation framework for accurate uwb antenna system design," *IEEE Internet of Things Journal*, vol. 12, no. 9, pp. 11 441–11 456, 2025.

[23] R. Wilssens, A. Lambrecht, G.-J. Gordebeke, S. Luchie, E. De Poorter, S. Lemey, and H. Rogier, "Towards Low-Cost and Resource-Efficient IEEE 802.15.4z-Compliant Ultra-Wideband Breathing Rate Estimation," in *2025 IEEE International Symposium on Antennas and Propagation and USNC-URSI Radio Science Meeting (APS/URSI)*, 2025.

[24] G. Quintero, J.-F. Zurcher, and A. K. Skrivervik, "System Fidelity Factor: A New Method for Comparing UWB Antennas," *IEEE Transactions on Antennas and Propagation*, vol. 59, no. 7, pp. 2502–2512, 2011.

[25] "IEEE Standard for Low-Rate Wireless Networks - Redline," *IEEE Std 802.15.4-2024 (Revision of IEEE Std 802.15.4-2020) - Redline*, pp. 1–967, 2024.